Chemical Science

ROYAL SOCIETY OF CHEMISTRY

EDGE ARTICLE

View Article Online
View Journal | View Issue

Cite this: *Chem. Sci.*, 2023, **14**, 10308

All publication charges for this article have been paid for by the Royal Society of Chemistry

Received 17th June 2023
Accepted 4th September 2023

DOI: 10.1039/d3sc03091a

rsc.li/chemical-science

The interface microenvironment mediates the emission of a semiconductor nanocluster *via* surface-dopant-involving direct charge transfer†

Zhiqiang Wang,‡[ab] Hao Ma,‡[a] Jiaxu Zhang,‡[ab] Yingjia Lan,‡[b] Jia-Xing Liu,[a] Shang-Fu Yuan,[a] Xiao-Ping Zhou,[a] Xiaohong Li,[b] Chaochao Qin,[c] Dong-Sheng Li[d] and Tao Wu*[ab]

The interface microenvironment of doped quantum dots (QDs) is crucial in optimizing the properties associated with the photogenerated excitons. However, the imprecision of QDs' surface structures and compositions impedes a thorough understanding of the modulation mechanism caused by the complex interface microenvironment, particularly distinguishing the contribution of surface dopants from inner ones. Herein, we investigated interface-mediated emission using a unique model of an atomically precise chalcogenide semiconductor nanocluster containing uniform near-surface Mn^{2+} dopants. Significantly, we discovered that Mn^{2+} ions can directly transfer charges with hydrogen-bonding-bound electron-rich alkylamines with matched molecular configurations and electronic structures at the interface. This work provides a new pathway, the use of atomically precise nanoclusters, for analyzing and enhancing the interface-dependent properties of various doped QDs, including chalcogenides and perovskites.

Introduction

Doped quantum dots (QDs) are widely used in solar cells,[1] photoelectric sensors,[2] and photocatalytic systems.[3] This is because of the intriguing optical, electronic, and catalytic properties of these nanostructures.[4–6] It has been demonstrated that the intentional doping of QDs creates new midgap/intermediate energy states, which can serve as energy/charge accepting centers and improve the intrinsic performance of the QDs and even result in new functionalities.[7–9] However, effectively manipulating the coupling interactions (*i.e.*, external and internal energy/charge transfer among the excitons in the photoexcited hosts, the dopants in the hosts, and the interfacial molecules attached to the hosts) while identifying their respective roles (*i.e.*, donor or acceptor) during these processes remains a challenge.[10–12] Early studies mainly focused on internal energy/charge transfer (IET/ICT) from the host to the dopants (or defects).[13,14] In the last decade, however, external energy/charge transfer (EET/ECT) between the host and interfacial molecules (IMs) has also been investigated because the interface microenvironment of QDs is essential for tuning the properties associated with the photoexcited excitons.[15] Nevertheless, there has been little research on the direct coupling interactions between the dopants and IMs, especially for the dopant-dominated direct ECT. This may be attributed to the following factors: (1) the dopants in QDs are usually randomly distributed within the QDs and/or on their surfaces (Scheme 1a), and a lack of precise information about the structure and location distribution of the dopants prevents an analysis of the above-described processes;[16] (2) ECT initiated by a small amount of surface dopants may be masked to a significant degree by EET arising from a large amount of inner dopants; (3) it is difficult to completely prevent surface vacant defects in QDs through surface passivation, making it challenging to study the excited-state dynamics of surface dopants (Scheme 1b); and (4) there exists an ambiguous interface microenvironment for QDs with an uneven surface, which usually obscures the bonding interactions with IMs.[17] Therefore, it is necessary to adopt atomically precise homogeneous doping models in order to overcome this research bottleneck.

In addition, organic amines play a significant role in the synthesis of QDs as well as in determining their

[a]*College of Chemistry and Materials Science, Guangdong Provincial Key Laboratory of Functional Supramolecular Coordination Materials and Applications, Jinan University, Guangzhou 510632, China. E-mail: wutao@jnu.edu.cn*

[b]*College of Chemistry, Chemical Engineering and Materials Science, Soochow University, Suzhou, Jiangsu 215123, China*

[c]*Henan Key Laboratory of Infrared Materials & Spectrum Measures and Applications, School of Physics, Henan Normal University, Xinxiang 453007, China*

[d]*College of Materials and Chemical Engineering, Hubei Provincial Collaborative Innovation Center for New Energy Microgrid, Key Laboratory of Inorganic Nonmetallic Crystalline and Energy Conversion Materials, China Three Gorges University, Yichang, Hubei 443002, China*

† Electronic supplementary information (ESI) available. See DOI: https://doi.org/10.1039/d3sc03091a

‡ These authors contributed equally.

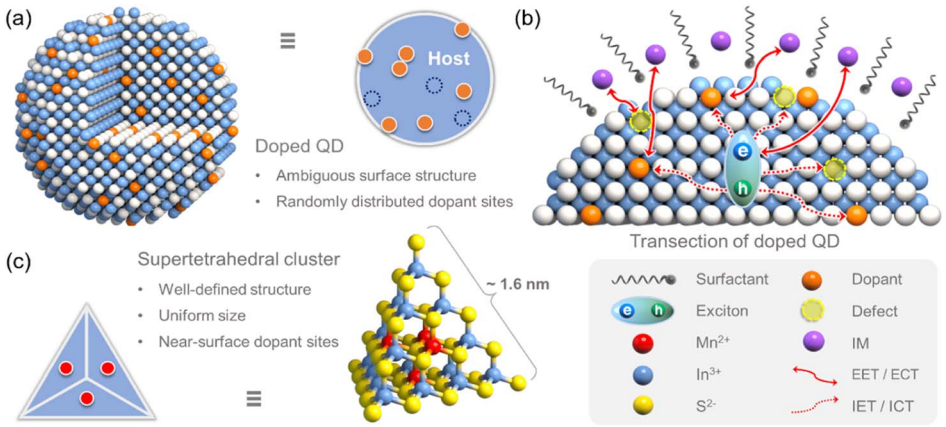

Scheme 1 (a) Schematic of a classical QD with randomly distributed dopant/defect sites. (b) Transection of a doped QD showing IET/ICT from the host to the dopant (or defect) and EET/ECT between the host (or dopant/defects at different sites) and IMs. (c) Structure of the atomically precise semiconductor model, namely, supertetrahedral T4-Mn clusters with Mn^{2+} ions uniformly distributed in the near-surface region (IET, internal energy transfer; ICT, internal charge transfer; EET, external energy transfer; ECT, external charge transfer; IM, interfacial molecule).

applicability.[18,19] Neutral organic amines and their derived cations are frequently employed for passivating (or modifying) the crystal surface of metal-chalcogenide- and halide-perovskite-based QDs.[20,21] In addition, organic amines are also used in photocatalytic reactions that occur at the surfaces/interfaces of QDs. For example, triethanolamine is used as a hole-sacrificing reagent to ensure high photocatalytic performance during the hydrogen evolution reaction as well as to improve the stability of the catalyst.[22] Furthermore, interfacial organic amine cations of halide-perovskite-based QDs can modulate the excited-state dynamics of the host. For example, Yang *et al.* reconfigured the near-edge state of perovskite QDs using organic amine cations with different degrees of steric hindrance and could effectively enhance the mobility of holes in the host material and improve the stability of the resulting devices.[23] Adachi *et al.* claimed that organic amine cations can quench the triplet energy of perovskites and hence reduce the emission efficiency of the triplet excitons.[24] Given these facts, we believe that an in-depth understanding of direct EET/ECT between dopants and interfacial amine molecules (or cations) would be beneficial for further understanding the modulation mechanism caused by the interface microenvironment and optimizing the performance of doped QDs for practical applications.

In this work, atomically precise T4-MnInS molecular nanoclusters ($[Mn_4In_{16}S_{35}]^{14-}$, denoted as T4-Mn in Scheme 1c), consisting of four uniformly distributed near-surface Mn^{2+} ions and thirty-four surface S^{2-} ions in a supertetrahedron, were employed as a model to study the direct coupling interactions between Mn^{2+} ions and IMs and specifically the direct ECT process with amine molecules.[25,26] To begin with, the photoluminescence (PL) properties of the surfactant-assisted T4-Mn dispersions were explored. This was followed by a study of the direct coupling interactions. The results of PL and ^1H nuclear magnetic resonance (NMR) spectroscopies, electrochemical characterizations, and femtosecond transient absorption measurements confirmed the occurrence of direct ECT between the Mn^{2+} ions and the interfacial neutral organic amines attached to the surfaces of the clusters *via* S···H–N hydrogen bonding. Furthermore, considering that the geometric configuration of amine molecules and their intrinsic electronic structure have a determining effect on their coupling strength, we also modulated the intensity of the Mn^{2+} emission by changing the interface microenvironment, *i.e.*, the coupling interactions of the clusters with different types of interfacial amines and other small molecules (*e.g.*, formamide and water).

Results and discussion

PL characteristics of T4-Mn crystals and dispersions

T4-Mn cluster-based microcrystals used here were synthesized and subsequently dispersed well in chloroform with the aid of the surfactant of dimethyldioctadecylammonium bromide (DODA·Br) (Fig. S1–S4†). T4-Mn dispersions (denoted as d_n, n = 0–6) with different surfactant/cluster molar ratios were prepared to optimize the dispersity of the clusters for the following investigation (see more details in the Experimental section and ESI†). Analyzing the PL characteristics of the clusters attached by the IMs would be an effective approach for probing the coupling interactions between the dopant and IMs.[27] To this end, we first determined the PL excitation (PLE) and PL spectra of the T4-Mn crystals and d_n dispersions. It can be seen from Fig. 1a that the Mn^{2+} emission from the T4-Mn crystals is attributable to a dominant indirect excitation pathway (*i.e.*, host-to-Mn^{2+} IET) and a secondary direct excitation one (*i.e.*, excitation of the Mn^{2+} ions).[28] Moreover, the Mn^{2+} emission from the T4-Mn crystals was centered at 604 nm for all the excitation wavelengths. The Mn^{2+} emission of dispersion d_0 exhibited a peak at 604 nm, which is the same as that of the T4-Mn crystals. However, the Mn^{2+} emissions of dispersions d_1–d_6 were slightly red-shifted compared with that of the T4-Mn crystals (the data on dispersion d_4 is shown in Fig. 1b and those of the others are in Fig. S5†); this may be ascribed to the pressure-induced strain experienced by the clusters because of

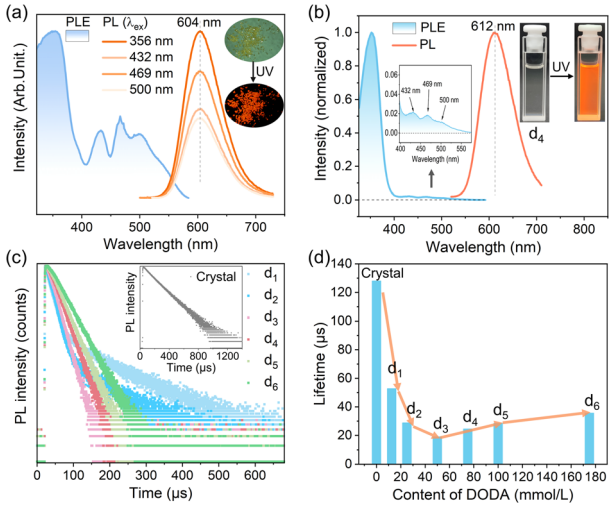

Fig. 1 (a) Steady-state PLE and PL spectra of T4-Mn crystals at various excitation wavelengths. (b) Steady-state PLE and PL spectra ($\lambda_{ex} = 356$ nm) of dispersion d_4. (c) PL decay curves of d_n dispersions. All decay curves correspond to maximum emission under excitation at 356 nm. (d) Histograms of average decay lifetimes of Mn^{2+} emission from d_n dispersions. Insets in (a) and (b) show optical photographs of T4-Mn crystals and dispersion d_4 under ambient and UV light, respectively. A magnified partial PLE spectrum is also shown in inset (b). Inset in (c) shows the PL decay curve of T4-Mn crystals.

the surrounding $DODA^+$ molecules (Fig. S6†). The PLE spectra of the dispersions were distinct from that of the T4 crystals (Fig. 1b and S5†), where the Mn^{2+} emission caused by the direct excitation of the Mn^{2+} ions was to some extent restricted. However, importantly, the direct-excitation properties of the Mn^{2+} ions in the dispersed clusters remained, similar to those of the clusters in the crystals. This may be caused by the aggregation of Mn^{2+} ions in the form of $[Mn_4S]$ units within the clusters, wherein the spin-coupling Mn···Mn interactions make the spin-prohibited d–d transition of the Mn^{2+} ions possible.[29] It is important to mention that this structure allows the Mn^{2+} ions in the clusters in the dispersion to be directly excited by visible light, thus facilitating the analysis of the direct coupling interactions between the IMs and Mn^{2+} ions.

To further elucidate the changes in the PL properties of the excited-state Mn^{2+} ions, the decay curves of the T4-Mn crystals and dispersions were measured at 365 nm (*i.e.*, the host clusters were excited) (Fig. 1c, d, and Table S1†). The T4-Mn crystals and dispersion d_0 exhibited single-exponential decay with emission lifetimes of ~128.0 (inset in Fig. 1c) and ~121.7 μs (Fig. S7†), respectively. In contrast, the PL decay modes for dispersions d_1–d_6 were different from those of each other, and their corresponding decay lifetimes were much shorter than those of the large-sized T4-Mn crystals and cluster-based NPs in dispersion d_0. The average lifetime of the Mn^{2+} emission from the surfactant-assisted dispersions initially decreased and then increased slightly with an increase in the amount of DODA·Br added (Fig. 1d). For dispersions d_1 and d_2, the decay curves of the Mn^{2+} emission could be fitted using a double-exponential function with a long component (similar to that of the T4-Mn crystals) and a short component (Table S1†). However, for dispersions d_3–d_6, the decay curves could be fitted using a single-exponential function, and their lifetimes increased slightly with an increase in the amount of DODA·Br used. Note that DODA·Br showed weak luminescence intensity and did not affect the Mn^{2+} emission measurements (Fig. S8†). Given the TEM results and the fact that the lifetimes of the Mn^{2+} emission of dispersions d_3–d_6 gradually increased with an increase in the amount of DODA·Br used, we concluded that the solvent molecules surrounding the clusters in the dispersions were responsible for the reduction in the emission lifetime, as collisions between these clusters and the chloroform molecules would consume the excited-state energy of the clusters and hence lower the PL lifetimes.[30] The long lifetime component of dispersion d_2 probably originates from the inner parts of the surfactant-encapsulated cluster-based nanoparticles (SENPs) (Fig. S2c†), which undergo negligible interactions with the chloroform molecules. Correspondingly, the outer parts of the SENPs exhibit strong interactions with the interfacial solvent molecules, resulting in the short lifetime component.[31] Owing to the single-exponential decay mode of dispersions d_3–d_6, we conjectured that each T4-Mn cluster in the 2–3 nm-sized SENPs interacts with the interfacial solvent molecules (Fig. S2d and e†). The presence of higher amounts of DODA·Br on the cluster surfaces partially prevents collisions between the clusters and solvent molecules, resulting in a slight increase in the Mn^{2+} emission decay lifetime. In addition, under the direct excitation of the Mn^{2+} ions, the Mn^{2+} emission intensity of dispersion d_4 increased with the addition of DODA·Br (Fig. S9†). This further confirmed that chloroform can directly quench the excited-state energy of the Mn^{2+} ions in the clusters to a certain extent.

Effects of interfacial neutral amine molecules on Mn^{2+} emission

Considering that the interfacial triplet oxygen ($^3O_2$) molecules close to QDs can quench the emission of the QDs,[32–34] control experiments were performed to investigate the possible coupling interactions of $^3O_2$ with the clusters (see more details in Fig. S10–S13† and the related description). Based on the observation of near-infrared PL of $^1O_2$, direct energy transfer from excited-state Mn^{2+} to $^3O_2$ proved to occur in this case. To further probe the coupling interactions between the clusters with organic IMs, PL measurements were performed on dispersion d_4 while adding other amine molecules, such as ethylenediamine (EDA) and triethylamine (TEA), to it (Fig. 2). The amine molecules were added in increasing quantities to a certain amount (3 mL) of the dispersion for qualitatively monitoring the variation in the Mn^{2+} emission with addition of the amines. The Mn^{2+} emission intensity decreased with the addition of the amines, with the trends for the two amines being different. The intensity of the Mn^{2+} emission decreased sharply with an increase in the amount of EDA, which has a linear structure, and was completely quenched when 50 μL of EDA was added (Fig. 2a). However, the decrease in the Mn^{2+} emission intensity was less rapid when the nonlinear-structured tertiary amine TEA was added (Fig. 2b). Fig. S14† shows the

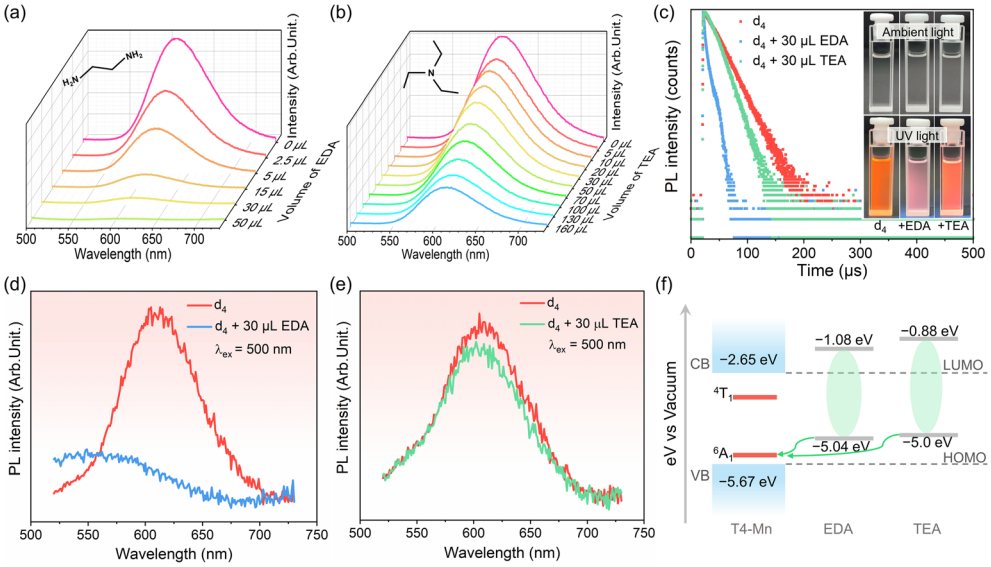

Fig. 2 (a and b) PL spectra of dispersion d_4 samples (3 mL samples were used) containing EDA and TEA in different amounts, respectively. (c) Decay curves of Mn^{2+} emission from dispersion d_4 before and after addition of 30 μL EDA and TEA (λ_{ex} = 356 nm and λ_{em} = 612 nm); the inset shows the optical images of dispersion d_4 samples with and without an amine added (30 μL of EDA and TEA) under ambient light and 365 nm excitation. (d and e) PL spectra of dispersion d_4 (λ_{ex} = 500 nm) with and without addition of 30 μL EDA and TEA, respectively. (f) Qualitative alignment of energy levels of clusters, EDA, and TEA, showing favored electron transfer from the HOMO level of amines to the ground state ($^6A_1$) of the Mn^{2+} ion.

Mn^{2+} emission intensity as a function of the amounts of EDA and TEA added. Finally, Fig. 2c shows the decay dynamics of the Mn^{2+} emission of d_4 with EDA and TEA added. The addition of EDA and TEA decreased the Mn^{2+} emission lifetime from 24.5 μs to 7.1 μs and 17.9 μs, respectively. Optical photographs of d_4 before and after the addition of amines are shown in the inset. These changes in the lifetimes are in line with changes in the Mn^{2+} emission intensity. Moreover, with the addition of the amines, dispersion d_4 exhibited a broad electron paramagnetic resonance signal (originating from the Mn–Mn coupling interactions within the clusters),[35] which was similar to that seen in the case of the pristine dispersion d_4 (Fig. S15†). This suggested that the amine molecules did not cause the collapse of the clusters.

The results described above confirmed the existence of coupling interactions between the T4-Mn clusters and the amine molecules. Mn^{2+} emission intensity is usually dependent on the host-to-Mn^{2+} IET efficiency or the newly formed relaxation pathways involving the excited Mn^{2+} ions.[36,37] To further elucidate the interface modulation mechanism of the Mn^{2+} emission owing to the addition of the amines, PL measurements were performed by directly exciting the Mn^{2+} ions. It is assumed that, in this situation, Mn^{2+} emission intensity would be directly related to the population of the excited-state Mn^{2+} ions and not the host clusters. Notably, under 500 nm excitation, the Mn^{2+} emission intensity decreased dramatically with the addition of EDA (Fig. 2d) but only slightly with the addition of TEA (Fig. 2e). The changes in the PL spectra were similar to those for the case where the Mn^{2+} ions were indirectly excited through host-to-Mn^{2+} IET. Based on this result, it was confirmed that direct coupling interactions had occurred between the Mn^{2+} ions and organic amines. Furthermore, according to UPS and electrochemical tests, the energy levels (Fig. 2f) of the cluster and amine molecules were determined to match each other for allowing direct electron transfer from EDA/TEA to excited Mn^{2+} ions (see more details in Fig. S16–S18† and the related description).

Hydrogen bonding between T4-Mn clusters and amine molecules

^{1}H-NMR measurements were performed to elucidate the interface microenvironment, *i.e.*, the interactions between the clusters and interfacial amine molecules. Given the abundant S^{2-} sites on the surfaces of the clusters, it was reasonable to assume that the hydrogen atoms on the N atom of the amines would form links with the surfaces of the clusters *via* hydrogen bonding.[38] This would cause the ^{1}H-NMR characteristics (chemical shift, integration intensity, or coupling splitting) of the H atoms on a given amine to change because of the formation of S···H–N hydrogen bonds.[39] A series of ^{1}H-NMR control experiments were performed on the amines, dispersion d_4, and their mixtures to confirm this (Fig. 3a and b). The ^{1}H-NMR spectrum of dispersion d_4 is shown in Fig. S2.† When EDA was added to the dispersion, the peak related to the $-NH_2$ group (2) at 1.17 ppm disappeared, and that related to the $-CH_2$ group (1) was downshifted from 2.75 to 2.73 ppm, with the shape of the peak also changing (Fig. 3a).[40] This indicated the formation of hydrogen bonds (N–H···S) between the dispersed clusters and EDA molecules. However, no obvious changes were detected in the ^{1}H-NMR signal of the TEA molecules in dispersion d_4 (Fig. 3b), suggesting that hydrogen bonds were not formed.[41] These results as well as the PL spectra and energy

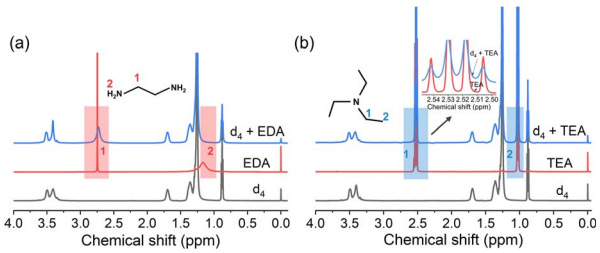

Fig. 3 (a) ^{1}H-NMR spectra of dispersion d_4, EDA, and their mixture. (b) ^{1}H-NMR spectra of d_4, TEA, and their mixture. $CDCl_3$ and tetramethylsilane were used as solvent and internal standard, respectively. Numbers in figures represent the H atom of a specific group. Inset in (b) shows magnified chemical peaks of the $-CH_2$ group (1).

levels indicated that the effect of the amines on the Mn^{2+} emission intensity may be related to their ability to form hydrogen bonds. The unbranched structure of the EDA molecule allows it to diffuse readily and pass through the surfactant molecules attached to the clusters. Thus, the EDA molecules can come close to the cluster surfaces (Scheme 2a); this is beneficial for forming hydrogen bonds and aids highly efficient ECT between the Mn^{2+} ions and EDA, thus resulting in the efficient quenching of the Mn^{2+} emission. In the case of the TEA molecules, the ^{1}H-NMR results indicated that they cannot form tight hydrogen bonds with the clusters (Scheme 2b), which is in keeping with the observation that the Mn^{2+} emission intensity was not reduced efficiently after the addition of TEA. Thus, it can be concluded that the coupling interactions between the Mn^{2+} ions and amines are dependent on the structural characteristics of the amine used. To ensure charge balance between the negatively charged clusters and positively charged $DODA^+$ ions, the $DODA^+$ ions should always be close to the clusters, which contained 35 surface S sites, owing to electrostatic interactions. However, the encapsulation phenomenon allows some of the clusters to form hydrogen bonds with the organic amines. It was expected that the coupling interactions between the Mn^{2+} ions and organic amines can be tuned by selecting an amine with the appropriate molecular structure.

Transient absorption (TA) spectra

Based on the results discussed above, we assumed that there must exist direct ECT between the near-surface Mn^{2+} ions in the clusters and the interfacial organic amine molecules. To further elucidate the underlying photophysical processes, ultrafast transient absorption spectroscopy was performed. A pump laser with a wavelength of 365 nm was used to excite the host clusters in d_4 samples with and without EDA, and the visible range of 400–650 nm was used for the probe beam. The time window was set to 7.39 ns. While the TA spectra of the surfactant-containing chloroform solution did not contain any positive excited-state-related absorption signals (Fig. S19†), those of dispersion d_4 did (Fig. 4a); these were attributable to the clusters in the dispersion. The relaxation of the excited-state absorption can be divided into two phases: a rapid phase and a slow one. The excited-state absorption spectrum decays rapidly initially (within 10 ps). However, in the subsequent stage, the decay rate was much slower, especially for the absorption band around 430 nm (Fig. 4a). Given the spin-forbidden nature of the $^4T_1 \rightarrow {}^6A_1$ transition of Mn^{2+},[42] it was assumed that the slower relaxation in the second stage was attributable to the excited-state energy level of the Mn^{2+} ions. Hence, the excited-state absorption relaxation with a longer delay time can be ascribed to the decay of the excited-state Mn^{2+} ions. A positive excited-state absorption signal was also observed after the addition of EDA (Fig. 4b). However, the rate of decrease of the fast-decay component was smaller, and the relaxation process during the

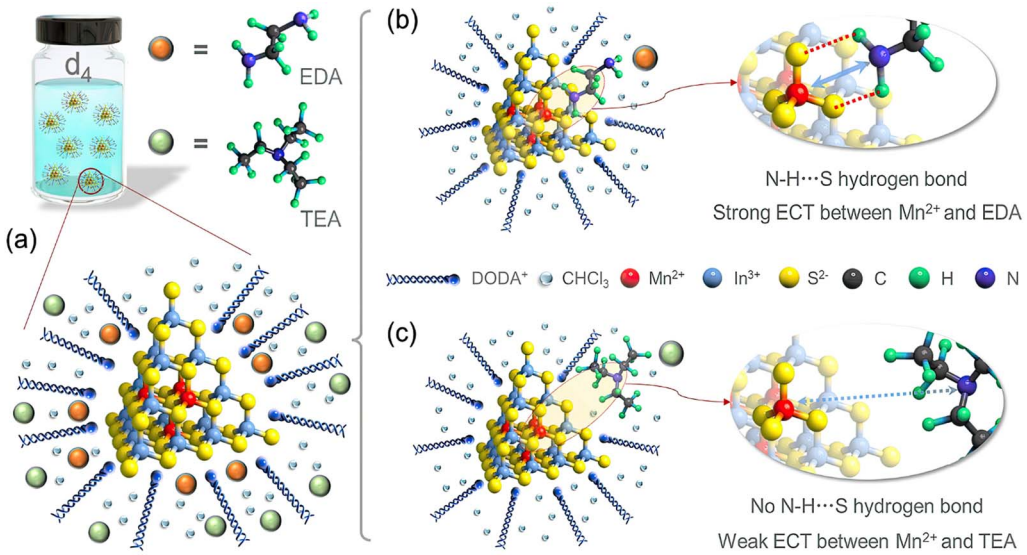

Scheme 2 Suggested hydrogen bonds between the cluster and amines. (a) Schematic of a single SENP in dispersion, showing the relative locations of EDA and TEA molecules close to a cluster surface. (b) Strong hydrogen bonding aids ECT between Mn^{2+} ions and EDA. (c) ECT between Mn^{2+} ions and TEA is not effective owing to the relatively long distance (no N–H···S hydrogen bonds formed).

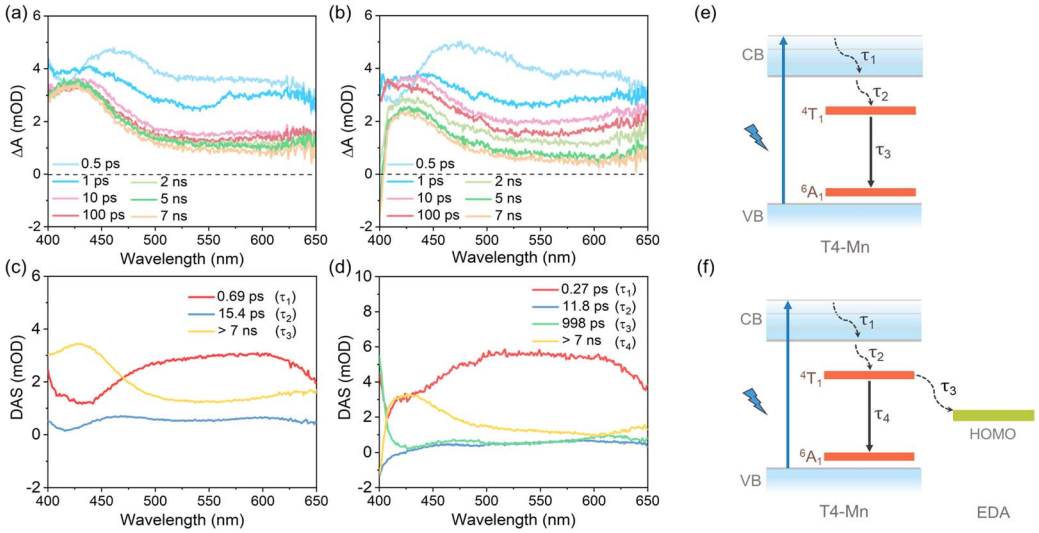

Fig. 4 fs-TA spectra (λ_{ex} = 365 nm) of dispersion d_4 (a) with and (b) without 30 μL EDA for several representative time delays. Decay-associated spectra (DAS) of dispersion d_4 (c) with and (d) without 30 μL EDA. (e and f) Schematic illustration of the photophysical mechanism with (e) and without (f) involving ECT between Mn^{2+} ions and EDA.

longer time window (of the order of nanoseconds) was a little faster compared with that of the pristine dispersion d_4 (*i.e.*, without EDA). This should be ascribed to the ECT between the excited-state Mn^{2+} ions and EDA, namely, electron transfer from the HOMO of EDA to the $^6A_1$ state of the Mn^{2+} ions (or hole transfer from the $^6A_1$ state of Mn^{2+} ions to the HOMO of EDA). Electron transfer from the HOMO level of EDA to the ground-state ($^6A_1$) of the Mn^{2+} ions is likely followed by synchronous electron transfer from the excited-state ($^4T_1$) of the Mn^{2+} ions back to the HOMO level of EDA for restoring the ground state of the amine molecules.[43]

Considering the decay kinetics corresponding to the different wavelengths with respect to the excited-state absorption spectrum, a global analysis was performed using Glotaran, a graphical user interface for the R-package TIMP (Vrije Universiteit Amsterdam, Amsterdam, Netherlands). The obtained decay-associated spectra (DAS) are shown in Fig. 4c and d. For dispersion d_4, three kinetics components were observed: 0.69 ps (τ_1), 15.4 ps (τ_2), and >7 ns (τ_3). According to the literature, the 0.69 ps component can be ascribed to internal conversion within the host from the high-lying excited state to the low-lying excited state, while the 15.4 ps component is related to a host-to-Mn^{2+} IET.[44–47] The >7 ns component is associated with the $^4T_1 \rightarrow {}^6A_1$ radiative transition and nonradiative pathways, in keeping with the results described above.[48] For the d_4 dispersion sample with EDA, four kinetics components were observed: 0.27 ps (τ_1), 11.8 ps (τ_2), 998 ps (τ_3), and >7 ns (τ_4). The 0.27 ps and 11.8 ps components were associated with the internal conversion process and the host-to-Mn^{2+} IET, respectively, as was also the case for the pristine d_4 dispersion. On the other hand, the third kinetics component of the pristine d_4 dispersion was divided into two components with time constants of 998 ps and >7 ns in the case of the d_4 dispersion sample with EDA. The >7 ns component was related to exciton recombination, including radiative and nonradiative Mn^{2+} ion decay. Thus, based on the results of this study and those reported previously, the 998 ps component can be ascribed to ECT between the Mn^{2+} ions and EDA.[49] The photophysical process is shown schematically in Fig. 4e and f. Essentially, electron transfer from the HOMO of EDA to the $^6A_1$ state of the Mn^{2+} ions is identical to hole transfer from the $^6A_1$ state of the Mn^{2+} ions to the HOMO of EDA. For the d_4 dispersion sample with TEA, there were no differences in the relaxation stages of the TA spectrum. In addition, a global analysis showed minor differences in the kinetics of the three components, with a weak ECT occurring between the Mn^{2+} ions and TEA in the case of the third component, which was difficult to dissociate (Fig. S20†).

Control of coupling interactions between Mn^{2+} ions and IMs

Based on the results described above, it can be concluded that the strength of the coupling interaction between the Mn^{2+} ions and amine molecules depends on the structure of the amines, as also shown in Scheme 2. Thus, proof-of-concept experiments were performed using several types of amines, including linear ones, such as ethanolamine (EA) and diethylenetriamine (DETA), and branched secondary amines, such as diethylamine (DEA). As expected, when the EA (or DETA) molecules were added into dispersion d_4, the Mn^{2+} emission (including its intensity and decay lifetime) decreased sharply, similar to the case for EDA (Fig. S21a, b, and d†). In the case of DEA, the decrease in the Mn^{2+} emission was lower and resembled that seen in the case of TEA (Fig. S21c and d†). Furthermore, on directly exciting the Mn^{2+} ions at 500 nm, a similar decrease in the Mn^{2+} emission intensity was detected (Fig. S22†). Finally, using optical and electrochemical measurements, direct ECT between the Mn^{2+} and the above amines was confirmed (Fig. S23–S27†). ^{1}H-NMR analysis also confirmed the formation of hydrogen bonds between the clusters and EA (or DETA)

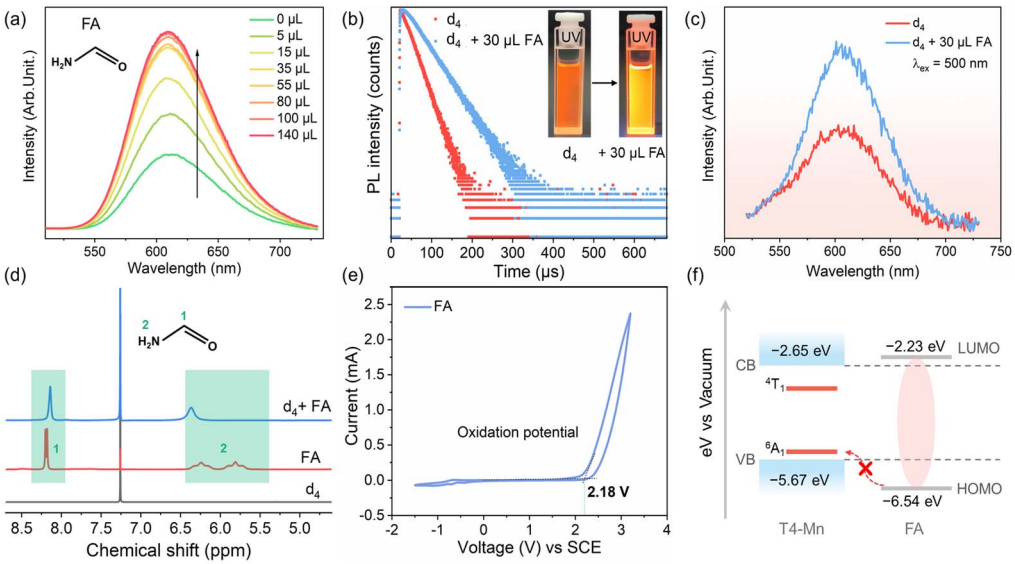

Fig. 5 (a) PL spectra of dispersion d_4 samples containing different amounts of FA. (b) PL decay lifetimes of d_4 before and after addition of 30 μL FA ($\lambda_{ex} = 356$ nm and $\lambda_{em} = 612$ nm). Inset shows optical images of d_4 samples with and without FA under ambient light and 365 nm excitation. (c) PL spectra of d_4 samples with and without FA ($\lambda_{ex} = 500$ nm). (d) ^{1}H-NMR spectra of d_4, FA, and their mixture formed using $CDCl_3$ as solvent. (e) CV curve of FA. (f) Qualitative energy level alignment of clusters and FA.

molecules but not with the DEA molecules (Fig. S28–S30†). The organic amines mentioned above are good electron donors. We wished to determine how Mn^{2+} emission would be affected if the electron-donating ability of the organic amine used were to be reduced. Thus, formamide (FA), which contains an electron-withdrawing carbonyl group, was used to investigate the coupling interactions with the clusters. With the addition of FA, both the Mn^{2+} emission intensity and decay lifetime increased (Fig. 5a and b). The results of electron paramagnetic resonance measurements confirmed the stability of the T4-Mn clusters after the addition of FA (Fig. S31†). This is the first report to suggest that the Mn^{2+} emission can be modulated using organic amines to realize PL turn-on behavior without having to modify the host clusters. Moreover, when the Mn^{2+} ions were excited directly, the intensity of the Mn^{2+} emission from the clusters increased after the addition of FA (Fig. 5c). To further elucidate the PL brightening mechanism, ^{1}H-NMR measurements were performed. Fig. 5d shows that the two groups of signals observed in the case of d_4 shifted with the addition of FA, and the doublet peaks (group 2, 5.8 ppm and 6.24 ppm) combined into a single one (6.36 ppm). The peak at 8.19 ppm shifted downfield to 8.14 ppm.[50] Hence, FA also formed hydrogen bonds with the clusters, resulting in an increase in the Mn^{2+} emission intensity. CV and relevant optical tests were performed to qualitatively analyze the enhancement in the Mn^{2+} emission intensity (Fig. 5e and S32†). The Förster resonance EET process was excluded, given the lack of spectral overlap. In addition, the oxidation potential of FA as determined from the CV curves is remarkably different from those of the other amines, owing to the poor electron-donating ability of FA. The energy levels of the clusters and FA are shown in Fig. 5f. Apparently, ECT did not occur between the clusters and FA as per the analysis above. Moreover, based on the fact that the excited Mn^{2+} ions may be de-excited because of the collisions of the clusters with the chloroform and $^3O_2$ molecules, we speculated that the increase in the PL intensity was caused by hydrogen bonding between the clusters and FA molecules, which prevented collisions between the clusters and the solvent molecules to a certain degree. Furthermore, it was found that the molecule of dimethylformamide with a structure similar to that of FA, that is, one in which the two H atoms on the N atom in FA were replaced by two $-CH_3$ groups, did not increase the Mn^{2+} emission intensity (Fig. S33†). This further confirmed the significance of interfacial hydrogen bonding in controlling the Mn^{2+} emission.

Based on the results described above, it can be concluded that the ability to form hydrogen bonds without aiding the ECT process with the clusters is responsible for the "turn-on" behavior of the PL from the Mn^{2+} ions. From a structural point of view, one of the most stable molecules, namely, H_2O, which consists of two H atoms attached to an O atom and is similar to the $-NH_2$ group, should readily form hydrogen bonds with the surface S sites of the clusters and thus enhance the Mn^{2+} emission intensity. To confirm this, we performed proof-of-concept experiments. Indeed, the Mn^{2+} emission properties of dispersion d_4, including the intensity and decay lifetime, increased with the addition of H_2O (Fig. S34†). In addition, the addition of H_2O can also recover the quenched Mn^{2+} emission of d_4 by EDA (Fig. S35†), which suggests H_2O molecules can strongly repel EDA molecules attached to the clusters.

Conclusions

In this work, the direct coupling interactions (energy and charge transfer processes) between Mn^{2+} ions and interfacial molecules were investigated systematically using well-defined

clusters of a chalcogenide semiconductor, T4-MnInS. The T4-MnInS clusters dispersed well in chloroform using the surfactant DODA·Br exhibited excited-state energy consumption, owing to the collisions between them (and the excited-state Mn^{2+} ions) and the chloroform molecules. Direct external energy transfer from the excited-state Mn^{2+} ions to the $^3O_2$ molecules, leading to the formation of $^1O_2$, was also confirmed. More importantly, using steady/transient-state optical measurements for the excited-state Mn^{2+} ions as well as electrochemical and ^{1}H-NMR analyses, direct external charge transfer between the Mn^{2+} ions and the interfacial organic amines was also demonstrated. It was found that the coupling strength between the Mn^{2+} ions and amines is dependent on the structure and electronic configuration of the amine in question. Based on this fact, the coupling interactions between the clusters and organic amines could be tuned. By rationally selecting an organic amine with poor electron-donating ability, the Mn^{2+} emission intensity could be increased by reducing the amount of energy consumed by the solvent molecules. This, in turn, allowed the PL "turn-on" effect to be realized in the case of other small molecules, such as H_2O. It is worth to be mentioned that current work is not easy to explore in the system of traditional Mn^{2+}-doped QDs. This work provides new insights into the interface-microenvironment-mediated coupling interactions (specifically, the direct external charge transfer process) that occur between well-defined, near-surface metal-doped clusters and interfacial molecules, which should help increase the applicability of metal-doped QDs in photophysical and optoelectronic devices.

Experimental section

Chemicals

Manganese acetate tetrahydrate ($Mn(Ac)_2\cdot 4H_2O$, AR, 99%) was purchased from Aladdin Industrial Corporation. Indium powder (In, 99.9%), dimethyldioctadecylammonium bromide (DODA·Br, 98%), and sublimed sulfur (S, 99.9%, powder) were supplied by Meryer Chemical Technology Co. Ltd. 2-(2-Aminoethylamino)ethanol (AEAE, ≥99%, liquid), 1,8-diazabicyclo [5.4.0]undec-7-ene (DBU, 99.0%, liquid), and hexamethyleneimine (98%, liquid) were purchased from Alfa Aesar company. Ethylenediamine (EDA, 99%, liquid), diethylenetriamine (DETA, 99%, liquid), ethanolamine (EA, 99%, liquid), triethylamine (TEA, >99.5%, liquid), and diethylamine (DEA, >99%, liquid) were commercially supplied by Macklin Biochemical Co. Ltd. Formamide (FA, ≥99.5%, liquid), *N*,*N*-dimethylformamide (DMF, 99%, liquid), chloroform (AR, 99%), acetonitrile (AR, 99%), and deionized water were supplied by National Pharmaceutical Group Corporation. All reagents and solvents were used as supplied without further purification.

Synthesis of T4-Mn crystals

The synthetic method of T4-Mn crystals was based on previous report with a slight modification.[51,52] Typically, $Mn(Ac)_2\cdot 4H_2O$ (61 mg, 0.25 mmol), indium powder (115.0 mg, 1.0 mmol), and sublimed sulfur (96.0 mg, 3.0 mmol) were mixed with AEAE (2.0 mL), DBU (1.0 mL), and hexamethyleneimine (1.5 mL) in a 23 mL Teflon-lining stainless steel autoclave, and stirred intensely for 0.5 h. The vessel was then sealed and heated up to 150 °C for 7 days, and then taken out from the oven and cooled naturally to room temperature. 50 mg of irregular micrometer-sized orange crystals were obtained after washing with ethanol several times and drying in air.

Synthesis of T4-Cd crystals

The synthesis method of T4-Cd crystals was similar to that of T4-Mn crystals with $Mn(Ac)_2\cdot 4H_2O$ (61.0 mg, 0.25 mmol) replaced by $Cd(Ac)_2\cdot 2H_2O$ (66.0 mg, 0.25 mmol). 60 mg of irregular micrometer-sized yellow crystals were finally obtained.

Preparation of T4-Mn dispersions (d_n, $n = 0$–6)

2.0 mg of T4-Mn crystals were mixed with different amounts (0 mg, 63 mg, 126 mg, 252 mg, 378 mg, 504 mg, and 882 mg) of surfactant DODA·Br, and then they were separately added into a glass vial with 8 mL of chloroform solvent, followed by magnetic stirring for 4 h, which accordingly resulted in the formation of T4-Mn dispersions with different concentrations of cluster and different concentration of DODA·Br (0 mmoL L^{-1}, 12.5 mmoL L^{-1}, 25 mmoL L^{-1}, 50 mmoL L^{-1}, 75 mmoL L^{-1}, 100 mmoL L^{-1}, and 175 mmoL L^{-1}) (denoted as d_0, d_1, d_2, d_3, d_4, d_5, and d_6, respectively). It was clearly observed that a larger amount of surfactant can lead to better dispersity of clusters. The crystals were found to be fully dispersed in chloroform when the amount of DODA·Br reached 378 mg, and a limpid dispersion was observed by the naked eye. However, the dispersions with a small amount of DODA·Br showed a turbid suspension. After centrifugation with a rotating rate of 8000 rpm for 4 minutes, the supernatants of dispersions were collected and used for subsequent study. Note: For all spectroscopic tests on dispersions throughout this work, 3 mL of dispersion was utilized.

X-ray diffraction (XRD)

Powder XRD measurements were carried out on medium-sized diffraction equipment (D2 PHASER, Bruker, Germany) with Cu Kα ($\lambda = 1.54056$ Å) radiation with 30 kV acceleration voltage and 10 mA working electric current.

Ultraviolet-visible spectroscopy (UV-Vis)

UV-Vis spectra were measured on a UV3600 UV-Vis-NIR spectrophotometer.

Transmission electron microscopy (TEM)

TEM measurements were carried out on an FEI TECNAI G2 F20 transmission electron microscope operated at 200 kV.

Ultraviolet photoelectron spectroscopy (UPS)

UPS measurements were performed on an Escalab 250Xi (Thermo Fisher Scientific) apparatus.

Cyclic voltammetry (CV)

CV measurements were carried out on a CHI 760e electrochemical analyzer with a three-electrode configuration at room temperature. An acetonitrile solution containing tetra-*n*-butylammonium perchlorate (0.1 M) was used as electrolyte. A glassy carbon electrode, Pt wire, and saturated calomel electrode (SCE) were employed as the working electrode, counter electrode, and reference electrode, respectively. The glassy carbon electrode was polished using 0.5 μm alumina powder, and rinsed with deionized water before CV tests. A scan speed of 100 mV s^{-1} was used during the working process. The CV curves of organic amines were calibrated with ferrocene/ferrocenium (Fc/Fc^+) as a standard tested under the same conditions. The energy level of Fc/Fc^+ was set to be −4.8 eV with respect to the vacuum level.

^{1}H-NMR

^{1}H-NMR spectra of dispersions were obtained from an Agilent DD2-600 instrument, and tetramethylsilane (TMS) was used as an internal standard.

Femtosecond transient absorption (fs-TA)

The fs-TA spectra were measured using a Helios pump–probe system. A 365 nm pulse laser was used as the pump beam, and visible light in the range of 400–650 nm was used as the probe beam. The time window was set to 7.39 ns.

Photoluminescence (PL)

Room-temperature steady-state PL and photoluminescence excitation (PLE) spectra were obtained on a HORIBA Scientific Fluorolog-3 fluorimeter equipped with a 450 W xenon lamp. PL decay data were recorded on a Fluorolog-3 spectrophotometer using a time-correlated single-photon counting (TCSPC) method.

Electron paramagnetic resonance (EPR)

Room-temperature X-band EPR spectra were obtained on a JES-X320 spectrometer with a 9.15 GHz magnetic field.

Data availability

All the data supporting this article have been included in the ESI.†

Author contributions

Z. Wang and T. Wu conceived and designed the project. Z. Wang, J. Zhang, Y. Lan, and J.-X. Liu synthesized the materials and carried out the PL, UV-Vis, UPS, CV, TEM, PXRD and EPR characterizations. Z. Wang, Y. Lan and X. Li performed ^{1}H-NMR characterization and analyzed the corresponding data. Z. Wang, J. Zhang and C. Qin performed TA measurements, and Z. Wang, H. Ma, J. Zhang, C. Qin, S.-F. Yuan, X.-P. Zhou, and D.-S. Li analyzed TA data. The manuscript was written through the contributions of all authors. All authors have approved the final version of the manuscript.

Conflicts of interest

There are no conflicts to declare.

Acknowledgements

The authors acknowledge financial support from the National Natural Science Foundation of China (No. 22071165 and 92261205) and the 111 Project (D20015).

References

1 P. K. Santra and P. V. Kamat, *J. Am. Chem. Soc.*, 2012, **134**, 2508–2511.
2 Q. Kong, B. Yang, J. Chen, R. Zhang, S. Liu, D. Zheng, H. Zhang, Q. Liu, Y. Wang and K. Han, *Angew. Chem., Int. Ed.*, 2021, **60**, 19653–19659.
3 W. Baek, D. R. Gamelin, M. S. Bootharaju, K. M. Walsh and T. Hyeon, *Nat. Mater.*, 2021, **20**, 650–657.
4 B. Su, G. Zhou, J. Huang, E. Song, A. Nag and Z. Xia, *Laser Photonics Rev.*, 2020, **15**, 2000334.
5 F. Meinardi, Q. A. Akkerman, F. Bruni, S. Park, M. Mauri, Z. Dang, L. Manna and S. Brovelli, *ACS Energy Lett.*, 2017, **2**, 2368–2377.
6 H. Zhang, J. Yu, C. Sun, W. Xu, J. Chen, H. Sun, C. Zong, Z. Liu, Y. Tang and D. Zhao, *J. Am. Chem. Soc.*, 2020, **142**, 16177–16181.
7 J. Jang, J.-K. Kim, J. Shin, J. Kim, K.-Y. Baek, J. Park, S. Park, Y. D. Kim, S. S. P. Parkin, K. Kang, K. Cho and T. Lee, *Sci. Adv.*, 2022, **8**, eabn3181.
8 M. Makkar, L. Dheer, A. Singh, L. Moretti, M. Maiuri, S. Ghosh, G. Cerullo, U. V. Waghmare and R. Viswanatha, *Nano Lett.*, 2021, **21**, 3798–3804.
9 K. R. Pradeep, A. Debdipto, J. Priyanka, G. Kushagra, Y. Anur, C. Andrea, Z. Margherita, C. Giulio, N. Chandrabhas and N. Shobhana, *ACS Energy Lett.*, 2019, **5**, 353–359.
10 E. Hofman, R. J. Robinson, Z. Li, B. Dzikovski and W. Zheng, *J. Am. Chem. Soc.*, 2017, **139**, 8878–8885.
11 R. D. Harris, S. B. Homan, M. Kodaimati, C. He, A. B. Nepomnyashchii, N. K. Swenson, S. Lian, R. Calzada and E. A. Weiss, *Chem. Rev.*, 2016, **116**, 12865–12919.
12 W. Lee, J. Oh, W. Kwon, S. H. Lee, D. Kim and S. Kim, *Nano Lett.*, 2019, **19**, 308–317.
13 B. Su, M. S. Molokeev and Z. J. Xia, *J. Phys. Chem. Lett.*, 2020, **11**, 2510–2517.
14 F. Muckel, S. Delikanli, P. L. Hernández-Martínez, T. Priesner, S. Lorenz, J. Ackermann, M. Sharma, H. V. Demir and G. Bacher, *Nano Lett.*, 2018, **18**, 2047–2053.
15 J. Wang, T. Ding, C. Nie, M. Wang, P. Zhou and K. Wu, *J. Am. Chem. Soc.*, 2020, **142**, 4723–4731.
16 S. Feldmann, M. K. Gangishetty, I. Bravić, T. Neumann, B. Peng, T. Winkler, R. H. Friend, B. Monserrat, D. N. Congreve and F. Deschler, *J. Am. Chem. Soc.*, 2021, **143**, 8647–8653.
17 Q. Wei, M. Li, Z. Zhang, J. Guo, G. Xing, T. C. Sum and W. Huang, *Nano Energy*, 2018, **51**, 704–710.

18 S. Mourdikoudis and L. M. Liz-Marzán, *Chem. Mater.*, 2013, **25**, 1465–1476.
19 P. R. Brown, D. Kim, R. R. Lunt, N. Zhao, M. G. Bawendi, J. C. Grossman and V. Bulovic, *ACS Nano*, 2014, **8**, 5863–5872.
20 B. Dhanabalan, G. Biffi, A. Moliterni, V. Olieric, C. Giannini, G. Saleh, L. Ponet, M. Prato, M. Imran and L. Manna, *Adv. Mater.*, 2021, **33**, 2008004.
21 D. P. Morgan and D. F. Kelley, *J. Phys. Chem. C*, 2018, **122**, 25661–25667.
22 J. Yang, D. Wang, H. Han and C. Li, *Acc. Chem. Res.*, 2013, **46**, 1900–1909.
23 J. Xue, R. Wang, X. Chen, C. Yao, X. Jin, K.-L. Wang, W. Huang, T. Huang, Y. Zhao, Y. Zhai, D. Meng, S. Tan, R. Liu, Z.-K. Wang, C. Zhu, K. Zhu, M. C. Beard, Y. Yan and Y. Yang, *Science*, 2021, **371**, 636–640.
24 C. Qin, T. Matsushima, W. J. Potscavage Jr, A. S. D. Sandanayaka, M. R. Leyden, F. Bencheikh, K. Goushi, F. Mathevet, B. Heinrich, G. Yumoto, Y. Kanemitsu and C Adachi, *Nat. Photonics*, 2020, **14**, 70–75.
25 J. Zhang, P. Feng, X. Bu and T. Wu, *Natl. Sci. Rev.*, 2022, **9**, nwab076.
26 J. Zhang, X. Bu, P. Feng and T. Wu, *Acc. Chem. Res.*, 2020, **53**, 2261–2272.
27 D. Li, C. Xu, Y. Liao, W. Cai, Y. Zhu and Z. L. Wang, *Sci. Adv.*, 2021, **7**, eabj0349.
28 Z. Wang, Y. Liu, J. Zhang, X. Wang, N. Chen, D. Li and T. Wu, *J. Mater. Chem. C*, 2021, **9**, 13680–13686.
29 X. Yang, C. Pu, H. Qin, S. Liu, Z. Xu and X. Peng, *J. Am. Chem. Soc.*, 2019, **141**, 2288–2298.
30 M. Zhu, Ji. Zhou, Z. Hu, H. Qin and X. Peng, *ACS Photonics*, 2018, **5**, 4139–4146.
31 C. Pu, J. Ma, H. Qin, M. Yan, T. Fu, Y. Niu, X. Yang, Y. Huang, F. Zhao and X. Peng, *ACS Cent. Sci.*, 2016, **2**, 32–39.
32 X. Dong, Y. Si, J. Yang, C. Zhang, Z. Han, P. Luo, Z. Wang, S. Zang and T. C. W. Mak, *Nat. Commun.*, 2020, **11**, 3678.
33 Y. Qian, D. Li, Y. Han and H. Jiang, *J. Am. Chem. Soc.*, 2020, **142**, 20763–20771.
34 R. Xu, Y. Wang, X. Duan, K. Lu, D. Micheroni, A. Hu and W. Lin, *J. Am. Chem. Soc.*, 2016, **138**, 2158–2161.
35 C. Xue, X. Fan, J. Zhang, D. Hu, Xi.-L. Wang, Xi. Wang, R. Zhou, H. Lin, Y. Li, D.-S. Li, X. Wei, D. Zheng, Y. Yang, K. Han and T. Wu, *Chem. Sci.*, 2020, **11**, 4085–4096.
36 K. Zhang, T. Yu, F. Liu, M. Sun, H. Yu, B. Liu, Z. Zhang, H. Jiang and S. Wang, *Anal. Chem.*, 2014, **86**, 11727–11733.
37 Y. Liu, J. Zhang, B. Han, X. Wang, Z. Wang, C. Xue, G. Bian, D. Hu, R. Zhou, D. Li, Z. Wang, Z. Ouyang, M. Li and T. Wu, *J. Am. Chem. Soc.*, 2020, **142**, 6649–6660.
38 J. Wu, B. Jin, X. Wang, Y. Ding, X.-L. Wang, D. Tang, X. Li, J. Shu, D.-S. Li, Q. Lin, Y.-B. Wu and T. Wu, *CCS Chem.*, 2021, **3**, 2584–2590.
39 Q. Zhang, R. Wang, B. Feng, X. Zhong and K. Ostrikov, *Nat. Commun.*, 2021, **12**, 6856.
40 N. S. Nudelman and C. E. S. Alvaro, *J. Phys. Org. Chem.*, 2011, **24**, 1067–1071.
41 H. E. Gottlieb, V. Kotlyar and A. Nudelman, *J. Org. Chem.*, 1997, **62**, 7512–7515.
42 N. Pradhan, *J. Phys. Chem. Lett.*, 2019, **10**, 2574–2577.
43 W. R. Algar, A. Khachatrian, J. S. Melinger, A. L. Huston, M. H. Stewart, K. Susumu, J. B. Blanco-Canosa, E. Oh, P. E. Dawson and I. L. Medintz, *J. Am. Chem. Soc.*, 2017, **139**, 363–372.
44 D. Luo, S. Yang, Q. Zhang, L. Cha, L. Dang and M. Li, *J. Phys. Chem. Lett.*, 2021, **12**, 1838–1846.
45 S. Wang, J. Leng, Y. Yin, J. Liu, K. Wu and S. Jin, *ACS Energy Lett.*, 2020, **5**, 328–334.
46 J. Yao, J. Ge, B. Han, K. Wang, H. Yao, H. Yu, J. Li, B. Zhu, J. Song and C. Chen, *J. Am. Chem. Soc.*, 2018, **140**, 3626–3634.
47 K. J. Babu, G. Kaur, A. Shukla, A. Kaur, T. Goswami, N. Ghorai and H. N. Ghosh, *J. Phys. Chem. Lett.*, 2020, **12**, 302–309.
48 R.-T. Liu, X.-P. Zhai, Z.-Y. Zhu, B. Sun, D.-W. Liu, B. Ma, Z.-Q. Zhang, C.-L. Sun, B.-L. Zhu, X.-D. Zhang, Q. Wang and H. L. Zhang, *J. Phys. Chem. Lett.*, 2019, **10**, 6572–6577.
49 D. Rossi, D. Parobek, Y. Dong and D. H. Son, *J. Phys. Chem. C*, 2017, **121**, 17143–17149.
50 R. J. Abraham, L. Griffiths and M. Perez, *Magn. Reson. Chem.*, 2013, **51**, 143–155.
51 Z. Wu, X. Wang, X. Wang, X. Xu, D. Li and T. Wu, *Chem. Eng. J.*, 2021, **426**, 131216.
52 X.-L. Wang, Z. Wu, X. Wang, C. Xue, C. Liu, J. Zhang, R. Zhou, D.-S. Li and T. Wu, *Electrochim. Acta*, 2021, **376**, 138048.